WIRELESS COMMUNICATIONS AND MOBILE COMPUTING
Wirel. Commun. Mob. Comput. 2016; **16**:3015–3031
Published online 30 September 2016 in Wiley Online Library (wileyonlinelibrary.com). DOI: 10.1002/wcm.2742

RESEARCH ARTICLE

High precision ranging with IR-UWB: a compressed sensing approach

Shaohua Wu[1,2], Ning Zhang[2*], Haibo Zhou[2], Qinyu Zhang[1] and Xuemin (Sherman) Shen[2]

[1] Shenzhen Graduate School, Harbin Institute of Technology, Harbin, China
[2] University of Waterloo, Waterloo, Canada

ABSTRACT

Ranging has been regarded as one of the fundamental enabling technologies for a multitude of applications that require high accurate position information, such as automated navigation, vehicle platooning, asset management, etc. Among various ranging techniques, impulse-radio ultra-wideband is one of the most competitive technologies for high-precision ranging, because of its capability of achieving centimeter-level ranging accuracy, even for dense urban, indoor or cave like environments. However, two main challenges arise when fully exploiting the ranging capability of impulse-radio ultra-wideband: (i) the extremely high sampling rate to acquire the received multipath signal, and (ii) the optimal thresholding strategy to differentiate the first path. To efficiently tackle those challenges, in this work, we propose a ranging approach under the compressed sensing framework. Specifically, the received ranging signal is acquired by low-rate compressed sampling through parallel random projections. Then, an algorithm named matching-pursuit search-back is proposed to detect the first arrival path, which integrates a backward iterative search and thresholding process starting from the peak path. The detection threshold is dynamically adjusted in each iteration to asymptotically minimize the averaged detection errors over false alarm and missed detection. Extensive simulations and experiments with field data are provided to demonstrate that the proposed approach can achieve high-precision ranging with far fewer samples compared with the traditional Nyquist-sampling based ones. Copyright © 2016 John Wiley & Sons, Ltd.

KEYWORDS
ranging; IR-UWB; compressed sensing; low-rate sampling

***Correspondence**
Ning Zhang, Department of Electrical and Computer Engineering, University of Waterloo, Waterloo, Canada.
E-mail: n35zhang@uwaterloo.ca

1. INTRODUCTION

Position information provision has rapidly become one of the fundamental prerequisites for many commercial, public safety, and military applications. Traditionally, position accuracy on the order of meters would be satisfactory for most of the applications, such as vehicle navigation, environmental monitoring, search and rescue location provision for mobile social networks, etc [1]. The most prevalently used positioning techniques for those applications are the global navigation satellite systems and wireless cellular systems [2]. However, in the foreseen future, we will witness the emergence of more and more applications requiring far more accurate position information. For example, meter-level positioning accuracy is needed for innovative applications in intelligent transportation systems [3]. For the next generation automated vehicle navigation systems, sub-meter accuracy is required to accomplish lane-level positioning and collision avoidance [4,5]. While for vehicle platooning [6] and some indoor applications such as asset management, even centimeter level accuracy is required. With GNNS or cellular positioning systems, the required highly accurate position information can hardly be achieved, especially in adverse environments where the line-of-sight ropagation of anchor node (i.e., the satellite or the cellular base station) signal is degraded or denied [7].

In order to accomplish the various levels of high positioning accuracy, one viable solution is to use ranges between non-anchor nodes (i.e., nodes with unknown position), either cooperatively with the existent positioning systems (GNNS or cellular systems) to augment the absolute positioning, or independently to conduct high precision relative positioning [8–10]. To obtain the range estimates, a variety of ranging approaches can be adopted, such as vision, ultrasonic, IrDA, Blue-tooth, ZigBee, WiFi, and impulse-radio ultra-wideband (IR-UWB). Among them, IR-UWB employs ultra-short radio frequency pulses (usually on the order of nanoseconds or even sub-nanoseconds)

Copyright © 2016 John Wiley & Sons, Ltd.

for ranging, with centimeter-level ranging accuracy in theory, and thus has been regarded as one of the most competitive technologies to realize high precision ranging between non-anchor nodes[11,12]. The high-precision ranging capability of IR-UWB essentially relies on its fine time resolution, which is promising to leverage time-of-arrival (TOA) estimation for ranging. Because the ultimate goal of TOA estimation is to precisely detect the first path from the received multipath signal, two main challenges have to be overcome for IR-UWB ranging: the requirement on high sampling rate and the difficulty in first path differentiation. According to the Shannon–Nyquist criterion, an analog-to-digital converter (ADC) with sampling rate on the order of 10 Giga-samples per second (Gsps) or even higher is needed for coherent first path detection [13–15], which is considerably difficult to implement at low cost and with low power. Moreover, because of the facts that non line-of-sight blockage may exist and the antennas may not be omnidirectional, the first path is not necessarily the strongest. Typically, thresholding strategies are adopted, but the optimal threshold selection should consider multiple factors, including the noise strength and the multipath channel characteristics.

To address the aforementioned challenges, in this paper, we first propose a low-rate compressed sampling scheme to acquire the received IR-UWB ranging signal based on the newly-emerging compressed sensing (CS) theory [16,17]. Different from the traditional low-rate point-sampling schemes, the proposed compressed sampling scheme allows the receiver digital back-end to reconstruct the high-resolution ranging waveform from the low-rate compressed samples. Then, to efficiently detect the first path, we propose a multi-metric threshold setting strategy, considering both the noise-related and channel-related factors. Specifically, the received multipath ranging signal is acquired through parallel multichannel random projections in the receiver analog front-end, with the projection interval specified to cover the region containing both the peak path (PP) and the first path. Then in the digital back-end, TOA estimation is directly performed upon the incoming low-rate compressed samples. Our proposed algorithm for detecting the first path, namely, matching-pursuit search-back (MP-SB), is actually a backward iterative shrinkage searching process starting from the PP. The threshold value used in MP-SB can be dynamically adjusted during each iteration to minimize the average detection error asymptotically.

The main contributions of this work are summarized as follows:

(1) We devise an analog front-end architecture for compressed sampling the IR-UWB ranging signal, which is structured by parallel multi-channel random projections.
(2) We design the MP-SB algorithms for TOA estimation from the low-rate compressed samples, which carries out an iterative backward search from the PP till the first path being detected.
(3) We propose a dynamic threshold setting strategy, jointly considering noise-related and channel-related factors, to asymptotically minimize the averaged error over false alarm and missed detection in each iteration of MP-SB.

The remainder of the paper is organized as follows. Section 2 provides the background and related works. The system model and problem statement are given in Section 3. In Section 4, detailed design of CS based ranging with IR-UWB is presented. The threshold setting strategy for first path detection is proposed in Section 5. Simulations and experiments with field data are presented in Section 6, followed by conclusions and future works in Section 7.

2. BACKGROUND AND RELATED WORKS

Impulse-radio ultra-wideband ranging relies on TOA estimation, and it can achieve centimeter level ranging accuracy in theory because of its ultra-fine time resolution. For applications that require highly accurate range or position information, such as vehicle platooning, indoor asset management, etc., ranging with IR-UWB has great potentials [11,12]. Taking the vehicle-to-vehicle ranging with IR-UWB as an example, shown in Figure 1, by estimating the signal propagation time τ_{prop}, the estimated range between the transmitter and receiver can be calculated as $\hat{d} = c \cdot \hat{\tau_{\text{prop}}}$, where c is the speed of electromagnetic wave, commonly known as $c = 3 \times 10^8$ m/s. The estimating process can be conducted either in the one-way ranging (OWR) manner or in the two-way ranging (TWR) manner. For OWR, at time t_0, the transmitter sends out one ranging pulse, which will arrive at the receiver via multiple paths. Among all the paths, the first path is usually the direct path, whose arrival time is denoted as t_1, and then the propagation delay can be calculated as $\tau_{\text{prop}} = t_1 - t_0$. A disadvantage of OWR is that t_0 and t_1 are recorded by two different clocks, that is, the transmitter clock and the receiver clock, and hence OWR is applicable only when the transmitter and receiver are time synchronized. While for TWR, the receiver will send back one response pulse to the transmitter at time t_2 after receiving the arrived ranging signal, with the processing delay $m = t_2 - t_1$ set in advance and known to both the transmitter and receiver. The response pulse will also arrive at the transmitter through multiple paths, with the arrival time of the first path denoted as t_3, so the two-way propagation delay can be calculated as $2\tau_{\text{prop}} = t_3 - t_0 - m$. Because both t_0 and t_3 are recorded by the transmitter clock, the TWR method can avoid the issue of transmitter-receiver synchronization.

Although OWR and TWR have different procedures, they both have to detect the first path from the received multipath signal to estimate the signal arrival time (i.e., t_1 for OWR, and t_1, t_3 for TWR), which is the main target of IR-UWB ranging systems. During the past decade, a lot of first path detection estimation algorithms were proposed

15308677, 2016, 17, Downloaded from https://onlinelibrary.wiley.com/doi/10.1002/wcm.2742 by University Of Waterloo, Wiley Online Library on [23/03/2026]. See the Terms and Conditions (https://onlinelibrary.wiley.com/terms-and-conditions) on Wiley Online Library for rules of use; OA articles are governed by the applicable Creative Commons License

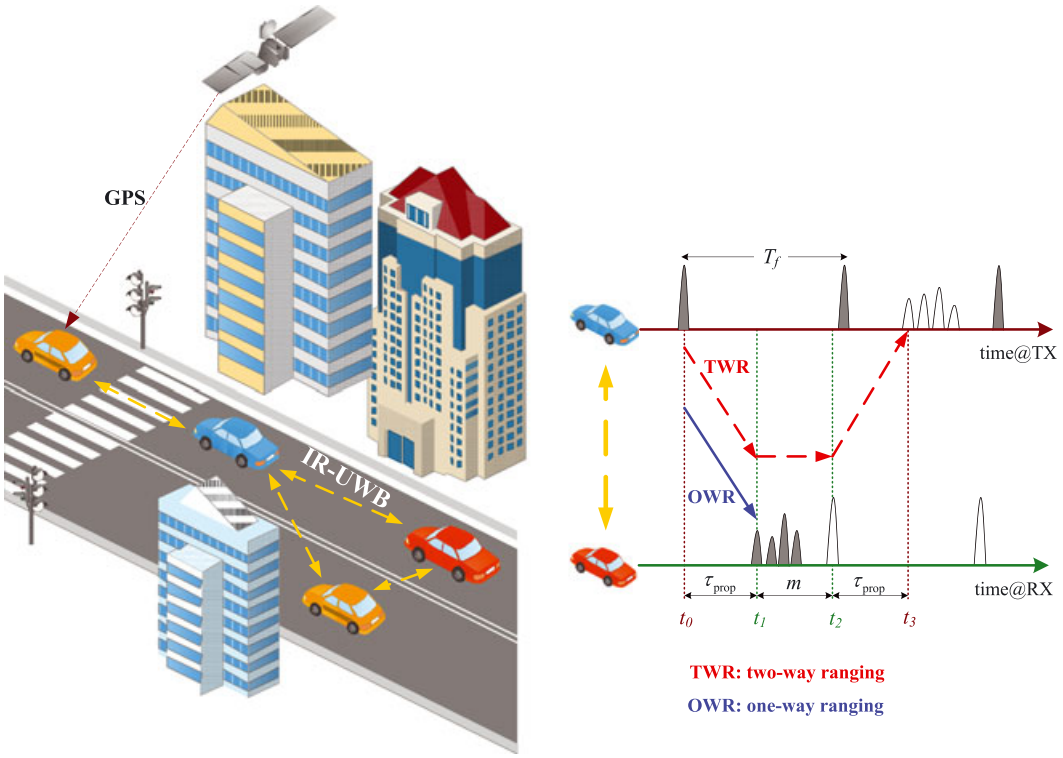

Figure 1. Illustration of vehicle-to-vehicle ranging with impulse-radio ultra-wideband (IR-UWB). GPS Global Positioning System; TX, transmitter; RX, receiver.

in the literature. According to the corresponding analog-part design, those algorithms can be mainly classified into coherent and non-coherent categories. The coherent algorithms are based on match-filtering or sliding correlation, thus can fully exploit the ranging ability of IR-UWB [13–15]. However, extremely high sampling rate on the order of 10 Gsps is required, which is considerably difficult to implement at low cost and with low power currently. As a tradeoff, some non-coherent algorithms which are mainly based on energy-detection are proposed, catering for practical low-cost ranging [18–21]. High-rate sampling is not required by energy-detection, but because of the coarse time granularity of low-rate energy samples, those non-coherent algorithms cannot fully exploit the capability of IR-UWB to achieve high-precision TOA estimates. As for the detection threshold setting in those algorithms, the adopted setting metrics are mainly noise-related, such as the noise strength, SNR, while channel-related factors are seldomly considered. In summary, because of the challenges with the signal sampling and threshold setting for first path detection, existing algorithms could not achieve the high performance.

The emerging theory of CS [16,17] provides a promising approach to address the sampling challenge. Some recent researches have shown the great potential of applying CS to the design of IR-UWB communication systems as well as IR-UWB radar systems. For example, CS is used to achieve high performance IR-UWB channel estimation by exploring the channel sparsity [22,23]; novel IR-UWB symbol detection strategies are designed under the CS framework [24–27] by exploring the transmitted signal sparsity; based on low-rate compressive measurements, new echo detection methods for IR-UWB radar imaging are proposed [28,29]. Taking into account the sparse character of narrowband interference in the frequency domain, CS-based narrowband interference mitigation methods are also proposed for IR-UWB communications [30]. Different from these works, in our work, CS is introduced to the IR-UWB ranging systems, aiming at providing a systematic solution for high-precision ranging with low-rate sampling. In addition, for the first path detection, a multi-metric threshold setting strategy is proposed, taking into account the effects of both noise and channel characteristics on ranging performance.

3. SYSTEM MODEL AND PROBLEM STATEMENT

As is mentioned in Section 2, the primary task of ranging with IR-UWB is to detect the first path from the received multipath signal. For ease of presentation, we take the OWR as the example. The system model is shown in Figure 2.

15308677, 2016, 17, Downloaded from https://onlinelibrary.wiley.com/doi/10.1002/wcm.2742 by University Of Waterloo, Wiley Online Library on [23/03/2026]. See the Terms and Conditions (https://onlinelibrary.wiley.com/terms-and-conditions) on Wiley Online Library for rules of use; OA articles are governed by the applicable Creative Commons License

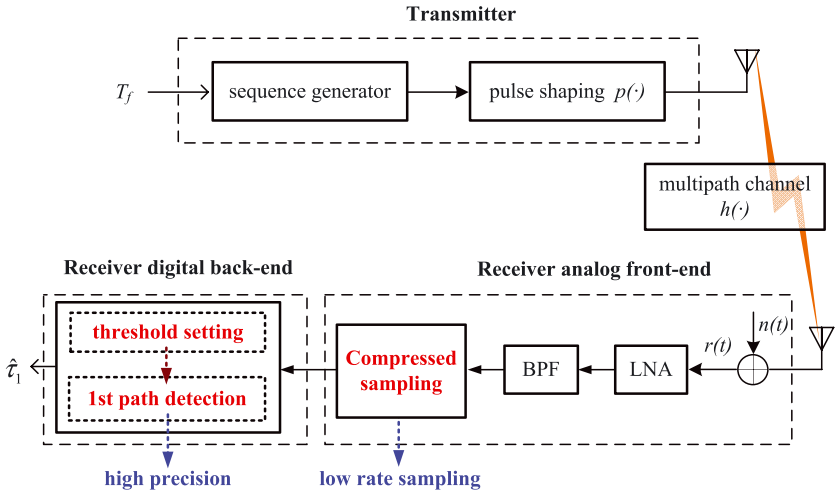

Figure 2. System model of compressed sensing based impulse-radio ultra-wideband ranging. BPF, band-pass filter; LNA,low-noise amplifier.

The ranging signal sent by the transmitter is a sequence of equally spaced pulses, which can be expressed as

$$s(t) = \sqrt{E_p} \sum_{j=0}^{N_f-1} p(t - jT_f) \tag{1}$$

where $p(t)$ denotes single pulse with unitary energy and duration T_p ; E_p denotes the transmitted pulse energy; N_f is the number of transmitted pulses; j and T_f are the pulse index and the frame duration, respectively.

The multi-path channel response is written as

$$h(t) = \sum_{i=1}^{L} a_i \delta(t - \tau_i) \tag{2}$$

where L is the number of propagation paths; a_i and τ_i are the attenuation and the delay of the ith path, respectively.

The received signal thus can be expressed as

$$r(t) = s(t) * h(t) + n(t) \tag{3}$$

where $n(t)$ denotes the additive white Gaussian noise (AWGN) with zero mean and two-sided power spectral density $N_0/2$; the variance of $n(t)$ is denoted as σ^2 .

On receiving the received signal, the receiver analog front-end conducts CS-based sampling and generate the low-rate compressed samples. By processing the incoming compressed samples, the receiver digital back-end detects the first path and estimates the arrival time.

Without loss of generality, we assume:

- Frame-level coarse acquisition is available, that is, the first path arrival time τ_1 in Equation (2) is less than T_f.
- T_f is set to be large enough to avoid inter-frame interference. Specifically, $T_f > T_{CIR} + \tau_1$, where T_{CIR} denotes the effective delay spread of the multi-path channel.
- The ranging channel is quasi-static, that is, $h(t)$ keeps unchanged within the duration of $N_f T_f$. Then the useful components within each frame of the received signal are the same, and the received data within the jth can be expressed as

$$\begin{aligned} r^{(j)}(t) &= \sqrt{E_p} \cdot p(t - jT_f) * h(t) + n^{(j)}(t) \\ &= \sqrt{E_p} \sum_{i=1}^{L} a_i p(t - jT_f - \tau_i) + n^{(j)}(t), \\ & t \in [jT_f,\ (j+1)T_f) \end{aligned} \tag{4}$$

where $n^{(j)}(t)$ is the intercepted segment of $n(t)$ within the jth frame, and E_p can be set as $E_p = 1$ for simplicity.

To estimate the TOA of the received signal, the parameter τ_1 in Equation (4) is required, which is correlated not only with the receiver analog front-end design, but also the digital back-end design. Specifically, three problems have to be solved to achieve the targeted low-rate sampling based high-precision ranging.

(1) In the receiver analog front-end, how to implement the CS-based sampling and get the low-rate compressed samples as the analog-part outputs?
(2) In the digital back-end, how to estimate the first path arrival time from the incoming low-rate compressed samples? That is, how to design the compressed sampling based first path detection algorithm.
(3) For the designed first path detection algorithm, how to guarantee its high performance? The performance is affected by both noise related and channel characteristic related factors. The detection threshold which is intended to differentiate the first path from the noise components and other arriving paths should be

15308677, 2016, 17, Downloaded from https://onlinelibrary.wiley.com/doi/10.1002/wcm.2742 by University Of Waterloo, Wiley Online Library on [23/03/2026]. See the Terms and Conditions (https://onlinelibrary.wiley.com/terms-and-conditions) on Wiley Online Library for rules of use; OA articles are governed by the applicable Creative Commons License

optimized so that the expected detection error can be minimized. In other words, how to set the threshold will affect the performance fundamentally.

In the next two sections, the aforementioned three problems will be addressed one by one to fulfill low-rate compressed sampling based high-precision ranging with IR-UWB.

4. COMPRESSED SENSING BASED SAMPLING AND THE FIRST PATH DETECTION ALGORITHM

In this section, we first briefly introduce the CS theory, and then give the detailed design of CS-based IR-UWB ranging receiver, including the analog front-end which conducts low-rate compressed sampling and the digital back-end where the first path detection algorithm is carried out to estimate the signal arrival time.

4.1. Compressed sensing preliminaries

The signal of interest $x \in \mathrm{R}^{N\times 1}$ is K-sparse on the basis (or dictionary) $\Psi = [\psi_1, \psi_2, \ldots, \psi_N]$, that is, $x = \sum_{n=1}^{N} \theta(n)\psi_n = \sum_{l=1}^{K} \theta(n_l)\psi_{n_l} = \Psi\theta$, where θ is an $N \times 1$ vector with K non-zero elements. To reconstruct x, we can linearly measure M (where $K < M \leq N$) projections of x on another basis Φ, that is, $y = \Phi x = \Phi\Psi\theta$. If $\Phi\Psi$ satisfies the restricted isometry property (RIP) [16], then x can be exactly reconstructed by solving the following problem:

$$\hat{\theta} = \arg\min \|\theta\|_1 \qquad \text{s.t.} \quad y = \Phi\Psi\theta \tag{5}$$

When Φ and Ψ are non-coherent, $\Phi\Psi$ satisfies RIP with high probability. Specifically, a randomly generated matrix Φ is non-coherent with any fixed matrix Ψ, thus a random matrix Φ is universally applicable.

In practical applications, the signal of interest is usually noisy, that is,

$$x = \Psi\theta + n_1 \tag{6}$$

where n_1 denotes the noise component such as AWGN. Distortion may also be introduced during the measurement process, that is, $y = \lfloor \Phi x \rceil_\Delta = \Phi x + n_2$ where $\lfloor\cdot\rceil_\Delta$ is the quantization operator, and n_2 denotes the quantization error. Therefore, the compressed samples are usually noise contaminated, which can be represented as $y = \Phi\Psi\theta + n$, where n is the equivalently composite noise. To reconstruct x from the noisy compressed samples, the following problem should be solved:

$$\hat{\theta} = \arg\min \|\theta\|_1 \qquad \text{s.t.} \quad \|y - \Phi\Psi\theta\|_2 \leq \varepsilon \tag{7}$$

where ε should be set according to the noise level.

Equation (5) is the traditional linear programming problem, and Equation (7) is the traditional second-order cone programming problem. Both of them can be solved by well-developed algorithms. Using slightly larger amount of measurements, greedy algorithms, such as matching pursuit (MP), orthogonal MP, and CoSaMP [31], can also be used to solve the two problems.

4.2. Receiver analog front-end: compressed sensing-based sampling

The prerequisite of applying CS is that the signal to be processed must be sparse in certain representation. In the following, we will first show that CS is appropriate for the IR-UWB ranging signal processing.

Let T_s' be a sufficiently small virtual sampling interval of the received signal. By virtual sampling, it means that this is only a "thought-experiment" construction, and no A/D conversion is done at rate $1/T_s'$. Because $T_{s'}$ actually represents the time resolution we expect on the reconstructed signal, it is usually set to be equal to or smaller than the Nyquist sampling interval. The virtual sampled form of Equation (4) is

$$\underline{r}^{(j)} = \underline{p} * \underline{h} + \underline{n}^{(j)} = \mathrm{P}^{(T_f, T_s')}\underline{h} + \underline{n}^{(j)} \tag{8}$$

where $\underline{p}$, $\underline{h}$, $\underline{n}^{(j)}$ denote the virtual sampled sequences of $p(t), h(t)$ and $n^{(j)}(t)$, respectively, with sequence length of $\lfloor T_f/T_s' \rfloor$; $\mathrm{P}^{(T_f,T_s')}$ is the equivalent circular matrix of $\underline{p}*$, with the convolution truncation length of $\lfloor T_f/T_s' \rfloor$. As for $\underline{h}$, only those elements indexed at $\lceil \tau_i/T_s' \rceil$ are non-zeros with values of a_i ($1 \leq i \leq L$). We can take a quick calculation to show that $\underline{h}$ is indeed sparse. For the commonly used IEEE 802.15.4a channel models [32], the 100 strongest paths are sufficient to characterize the channel and can collect the majority of the multipath energy, so $L \approx 100$; set $T_f = 200$ ns and $T_s' = 0.05$ ns, then the length of $\underline{h}$ is $\lfloor T_f/T_s' \rfloor = 4000$. It is obvious that $L \ll \lfloor T_f/T_s' \rfloor$. In all, it can be observed that Equation (8) accords perfectly with the noisy sparse signal model presented by Equation (6) (with $\mathrm{P}^{(T_f,T_s')}$ mapping to Ψ and $\underline{h}$ mapping to θ), thus the IR-UWB ranging signal can be low-rate sampled under the CS framework.

To implement CS based low-rate sampling, the ultimate goal is to design an analog structure that plays the role of the matrix Φ in Equations (5) and (7). Additionally, the resulting composite matrix $\Phi\mathrm{P}^{(T_f,T_s')}$ should satisfy the RIP so that information of the ranging signal to be acquired is preserved. Because a random matrix Φ is universally applicable, random filtering [33] or random demodulating [34] based analog structure can be used. In this work, we present a parallel multi-channel random demodulating architecture to sample the received ranging signal. As shown in Figure 3, there are M_e parallel channels linearly projecting the received signal. Any waveform randomly generated according to a Gaussian, Bernoulli, or more generally any sub-Gaussian distribution can be used as the projection waveform for each channel. Among the various types of randomly generated waveform, the Bernoulli

15308677, 2016, 17, Downloaded from https://onlinelibrary.wiley.com/doi/10.1002/wcm.2742 by University Of Waterloo, Wiley Online Library on [23/03/2026]. See the Terms and Conditions (https://onlinelibrary.wiley.com/terms-and-conditions) on Wiley Online Library for rules of use; OA articles are governed by the applicable Creative Commons License

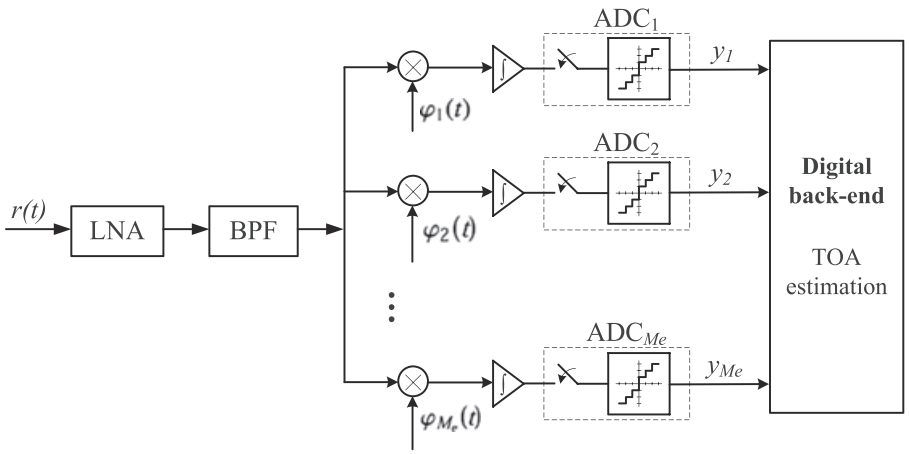

Figure 3. Illustration of compressed sampling of the received impulse-radio ultra-wideband ranging signal. ADC, analog-to-digital converter; BPF, band-pass filter; LNA, low-noise amplifier; TOA, time-of-arrival.

sequence is the easiest for implementation because it can be generated by a pseudo random number generator. In addition, the performance difference between different types of sub-Gaussian waveforms is negligible. Therefore, the proposed sampling structure adopts pseudo random noise as the measurement waveform, that is, $\varphi_m(t)$ $(m = 1, 2, \cdots, M_e)$ is a pseudo random noise sequence with chip rate of $1/T_s'$. For hardware implementation, the pseudo random noise sequence can be generated by linear feedback shift registers. The virtual sampled sequence of $\varphi_m(t)$ then corresponds to the row elements of the compressed sampling matrix Φ. The projection interval is denoted as $[t_{start}, t_{start} + T_{prj}]$, where t_{start} is the offset of the projection start point relative to the frame start point, and T_{prj} is the projection length; the sampling interval of the ADC is T_f, with $T_f \geq T_{prj}$. In the following, we will elaborate how to set the projection interval and details of the compressed sampling process.

4.2.1. The projection interval setting.

Because the essence of TOA estimation is to detect the first path, the projection interval does not need to cover the entire frame. Instead, we can choose a shorter signal segment where the first path is contained with satisfactory high probability as the projection interval. By doing so, the signal dimension is reduced from $\lfloor T_f/T_s' \rfloor$ to $\lfloor T_{prj}/T_s' \rfloor$, and thus the requirement on the number of measurements is also relaxed. Moreover, the data amount input to the digital back-end is reduced, consequently reducing the computational complexity.

The reference point to determine the projection interval is the PP of the received signal, which can be located by peak detection. The first path will be covered by tracing back long enough from the PP, that is, the projection interval can be set as $[\tau_{peak} + T_p T_p 2 - T_{prj}, \tau_{peak} + T_p/2]$, where the half pulse length after the peak point is also covered so that the entire PP can be projected. Let $\delta = \tau_{peak} - \tau_1$ denote the arrival time difference between the first path and the PP, then T_{prj} can be set large enough so that $\Pr\left(\delta \leq T_{prj} - \frac{T_p}{2}\right) \to 1$.

4.2.2. Compressed sampling.

The signal segment falling within the projection interval is,

$$\underline{r}_{prj}^{(j)} = \underline{p} * \underline{h}_{prj} + \underline{n}_{prj}^{(j)} = \mathrm{P}^{(T_{prj}, T_s')} \underline{h}_{prj} + \underline{n}_{prj}^{(j)} \tag{9}$$

The length of each virtual sampled sequence in Equation (9) is $\lfloor T_{prj}/T_s' \rfloor$, and $\mathrm{P}^{(T_{prj}, T_s')}$ denotes the convolution matrix with truncation length of $\lfloor T_{prj}/T_s' \rfloor$. Compressed sampling on $\underline{r}_{prj}^{(j)}$ will generate M_e measurements. Let M denote the required number of measurements for precise ranging, to reduce the number of projection channels and hence reduce the hardware cost, the overall M times of measuring can be distributed to D consecutive frames, that is, $M = D \cdot M_e$. Therefore, there are $N_D = N_f/D$ batches of compressed measurements, and the nth batch of measurements can be represented as

$$y[n] = \left[y^{(1)}[n], y^{(2)}[n], \cdots, y^{(D)}[n] \right]^T \tag{10}$$

where $y^{(d)}[n] (1 \leq d \leq D)$ denotes the M_e measurements corresponding to the dth signal frame in the nth batch. $y^{(d)}[n]$ can be written as follows:

$$\begin{aligned} y^{(d)}[n] &= \Phi_{(n,d)} \underline{r}_{prj}^{((n-1)D+d)} \\ &= \Phi_{(n,d)} \mathrm{P}^{(T_{prj}, T_s')} \underline{h}_{prj} + \Phi_{(n,d)} \underline{n}_{prj}^{((n-1)D+d)} \end{aligned} \tag{11}$$

where $\Phi_{(n,d)}$ denotes the measurement matrix composed by the virtual sampled sequence of the M_e measurement waveforms, $\varphi_m^{(n,d)}(t) (m = 1, 2, \cdots, M_e)$, and it is the submatrix of the equivalent compressed sampling matrix. The measurement waveforms adopted for different batches do

15308677, 2016, 17, Downloaded from https://onlinelibrary.wiley.com/doi/10.1002/wcm.2742 by University Of Waterloo, Wiley Online Library on [23/03/2026]. See the Terms and Conditions (https://onlinelibrary.wiley.com/terms-and-conditions) on Wiley Online Library for rules of use; OA articles are governed by the applicable Creative Commons License

not vary, that is, $\varphi_m^{(n,d)}(t)$ does not vary with n. Thus $\Phi_{(n,d)}$ can be simply denoted as $\Phi_{(d)}$. Because the statistical characteristics of the noise components within each frame are the same, without influencing the performance analysis results, $\underline{n}_{prj}^{((n-1)D+d)}$ can be simply denoted as $\underline{n}_{prj}$. Let $\Phi = \left[\Phi_{(1)}^T|\Phi_{(2)}^T|\cdots|\Phi_{(D)}^T\right]^T$, then Φ is just the equivalent compressed sampling matrix. Equation (10) can be expressed as

$$y[n] = \Phi \mathrm{P}^{(T_{prj},T_s')}\underline{h}_{prj} + \Phi\underline{n}_{prj} \tag{12}$$

The first non-zero of $\underline{h}_{prj}$ in Equation (12) just corresponds to the center of the first path. Therefore, to estimate the TOA under CS framework, we only need to locate the first non-zero in $\underline{h}_{prj}$ based on the noisy compressed samples in Equation (12). Usually, a processing gain could be obtained by taking average over the N_D batches of measurements, that is,

$$\bar{y} = \frac{1}{N_D}\sum_{n=1}^{N_D} y[n] = \Phi \mathrm{P}^{(T_{prj},T_s')}\underline{h}_{prj} + \Phi\bar{\underline{n}}_{prj} \tag{13}$$

where $\bar{\underline{n}}_{prj}$ denotes the virtual sampled AWGN sequence with variance of $\sigma_{avg}^2 = \sigma^2/N_D$.

4.3. Receiver digital back-end: first path detection

By compressed sampling, all information is now preserved in the sampled results in Equation (13). To estimate the TOA of the received signal, it requires the estimation of first path center location, that is, the index of the first non-zero element of $\underline{h}_{prj}$ in Equation. (13). In what follows, we concentrate on the algorithm design for first path detection.

4.3.1. A simple and direct strategy.

A simple and direct strategy is to fully reconstruct $\underline{h}_{prj}$ first, and then apply threshold comparison on $\hat{\underline{h}}_{prj}$. Those algorithms in the literature to solve the second-order cone programming problem, such as MP, orthogonal MP, and CoSaMP, can be used for reconstruction. However, the essence of TOA estimation is to locate the first path, not to reconstruct all the paths. Therefore, the number of measurements needed can be decreased, and consequently the computational complexity will also be reduced. To this end, we propose the following MP-SB algorithm.

4.3.2. The matching-pursuit search-back algorithm.

Before presenting the details of the proposed algorithm, we first clarify the terms and parameters in Figure 4.

- *Peak path:* the strongest path of the arrived multipaths, that is, the path that needs to be locked before setting the projection interval.
- *Tip path (TP):* the strongest path within a certain region left to PP. More specifically, "tip path 1" is the strongest path left to PP, that is, the strongest path within the region $\left[\tau_{peak} + T_p/2 - T_{prj}, \tau_{peak}\right)$; "tip path 2" is the strongest path left to "tip path 1", that is, the strongest path within the region $\left[\tau_{peak} + T_p/2 - T_{prj}, \tau_{TP\_1}\right)$, where τ_{TP_1} denotes the arrival time of "tip path 1". The last TP is just the first path, whose arrival time is the TOA to be estimated.
- *Falling times:* the index of a TP relative to PP, denoted by ξ. Specially, the falling times of the last TP, also the first path, is denoted as ς.

Taking $\underline{h}_{prj}$ in Figure 4 as an example, we can see that there are three TPs in total, and "tip path 3" is also the "first path", with $\xi = 3$ and $\varsigma = 3$.

The proposed algorithm is based on MP with backward search, whose main idea is as follows. A backward iterative shrinkage search is started from the PP to find out the TPs one by one through MP. During each iteration, the relative amplitude, that is, the ratio of TP's amplitude to PP's, is compared with a dynamic threshold. If the relative amplitude is larger than the threshold, the iterative search continues; otherwise, the iteration stops, and the last found TP is regarded as the first path.

Let t denote the iteration times of the TOA estimation algorithm, $\rho = |a_{TP}/a_{PP}|$ represent the relative amplitude, $\omega^2 = \sigma_{avg}^2/a_{PP}^2$ represent the relative noise power, and θ_ρ denote the detection threshold. θ_ρ is adaptively adjusted during each iteration, according to multiple factors, including the current iteration times, the relative noise power, the relative amplitude and the location of the previous found TP. The method of calculating θ_ρ for each iteration will be discussed in next section. Details of the proposed MP-SB TOA estimation algorithm is given as follows:

(1) Initialization. Let $V = \Phi \mathrm{P}^{(T_{prj},T_s')}$ denote the dictionary matrix, and v_i $(1 \le i \le N)$ correspond to the ith column of V, that is, the ith atom in the dictionary. The residual is initialized as $e_0 = \bar{y}$, and the initial search region ends at $l_0 = N + 1$, so that the right boundary of the projection interval is covered. The iteration times is initialized as $t = 0$, and the channel response estimation is initialized as $\hat{\underline{h}}_{prj} = 0^{N\times 1}$.

(2) Let $t = t + 1$, find the atom in the dictionary that matches the residual best, that is,

$$l_t = \underset{1\le i<l_{t-1}}{\arg\max} \frac{|\langle e_{t-1}, v_i\rangle|}{\|v_i\|} \tag{14}$$

(3) Estimate the coefficient of the found atom, that is, the amplitude of the corresponding path. If $t = 1$, the found path is PP; otherwise, the found path is TP.

$$\hat{\underline{h}}_{prj}(l_t) = \hat{\underline{h}}_{prj}(l_t) + \frac{|\langle e_{t-1}, v_i\rangle|}{\|v_i\|^2} \tag{15}$$

15308677, 2016, 17, Downloaded from https://onlinelibrary.wiley.com/doi/10.1002/wcm.2742 by University Of Waterloo, Wiley Online Library on [23/03/2026]. See the Terms and Conditions (https://onlinelibrary.wiley.com/terms-and-conditions) on Wiley Online Library for rules of use; OA articles are governed by the applicable Creative Commons License

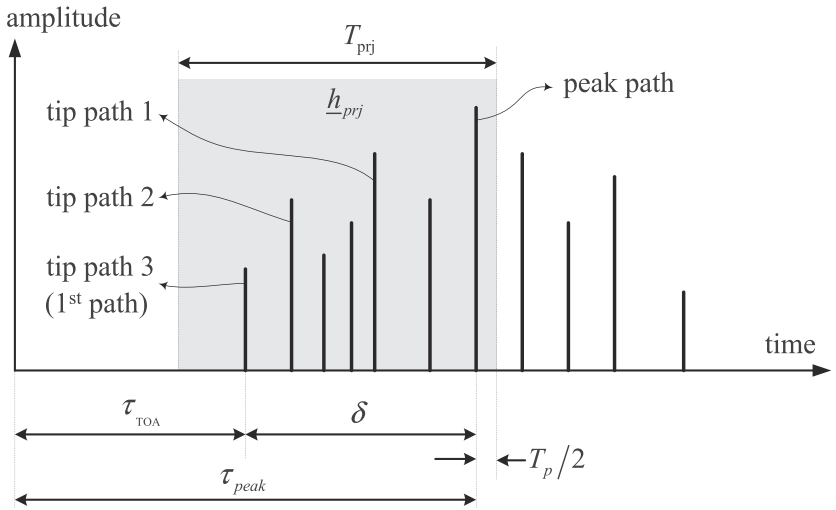

Figure 4. Illustration of $\underline{h}_{prj}$.

$$\hat{\rho} = \left| \hat{\underline{h}}_{prj}(l_t) \Big/ \hat{\underline{h}}_{prj}(l_t) \right| \tag{16}$$

(4) If $t = 1$, then set θ_ρ=0; otherwise, calculate the value of θ_ρ. The information used for calculation includes the current iteration times, the results of previous iteration, that is, the relative amplitude and location of the previous found TP, and the relative noise power, that is, $\omega^2 = \sigma^2_{avg} / \left(\hat{\underline{h}}_{prj}(l_1) \right)^2$.

(5) If $\hat{\rho} < \theta_\rho$, then stop the iteration and jump to step 6; otherwise, update the residual as

$$e_t = e_{t-1} - \frac{|\langle e_{t-1}, v_i \rangle|}{\|v_i\|^2} v_{l_t} \tag{17}$$

Then, go to step 2 to continue to find other TPs in the region left to the previous found TP.

(6) TOA is estimated as $\hat{\tau}_{TOA} = (l_{t-1} - 1) \cdot T'_s + \tau_{peak} + T_p/2 - T_{prj}$.

5. THRESHOLD SETTING FOR THE FIRST PATH DETECTION ALGORITHM

The setting of θ_ρ for the proposed MP-SB algorithm greatly affects the estimation performance. The optimal threshold setting strategy should minimize the first path detection error, which are determined by two categories of factors: noise related and channel characteristics related factors. In this section, we first take detailed analysis of the detection error of MP-SB, by jointly considering all different kinds of factors. Then the threshold setting strategy is proposed to asymptotically minimize the detection error. A case study using the IEEE 802.15.4a channel modes are given for further understanding of the proposed strategy.

5.1. Error analysis for matching-pursuit search-back algorithm

From the procedure of MP-SB, we can see that the following metrics will affect final detection performance: the relative noise power, that is, $\omega^2 = \sigma^2_{avg} / \left(\hat{\underline{h}}_{prj}(l_1) \right)^2$, and metrics that can characterize the channel property, including the first path falling times, that is, ς, the TP falling times, that is, ξ, the relative amplitude of TP to PP, that is, ρ, and the arrival time difference of first path to PP, that is, δ. Let $\Pr(\varsigma)$ denote the distribution of the first path's falling times, with $\varsigma = 0$ representing the situation that the first path is also the PP. Let $f_\delta(\delta|\varsigma)$ denote the distribution of δ under different ς, and $f_\rho(\rho|\xi)$ denote the distribution of ρ under different ξ. Next, we will use these metrics to derive the error of MP-SB.

Two cases may occur when the MP-SB algorithm is executed. One is the non-derailment case, where the search process will not derail from the track "SP→ TP1→ TP2→ first path $\cdots$". This is also the expected ideal case, because each iteration can successfully locate the corresponding tip path. The other is the derailment case, where components other than SP or TP are found by the algorithm. Here, we firstly concentrate on the non-derailment case. For the tth iteration, the non-optimal setting of θ_ρ may result in two kinds of detection errors: the false alarm and the missed detection.

5.1.1. False alarm error.

The first path has already been found in the $(t-1)$th iteration, that is, $\varsigma = t - 2$. During the tth iteration, the matched atom actually corresponds to a noise component. Therefore, $\hat{\rho} = |\rho_n|$, where the relative amplitude of noise ρ_n is Gaussian distributed with zero mean and variance of $\omega^2 = \sigma^2_{avg}/a^2_{PP}$. If $\theta_\rho < \hat{\rho}$, then the iteration continues, and the final detection corresponds to certain location

15308677, 2016, 17, Downloaded from https://onlinelibrary.wiley.com/doi/10.1002/wcm.2742 by University Of Waterloo, Wiley Online Library on [23/03/2026]. See the Terms and Conditions (https://onlinelibrary.wiley.com/terms-and-conditions) on Wiley Online Library for rules of use; OA articles are governed by the applicable Creative Commons License

within the region $[1, l_{t-1})$, resulting in false alarm error. Let $\vartheta(i)$ denote the i.i.d. Gaussian process with state distribution the same as ρ_n, the probability of false alarm can be derived as follows,

$$\begin{aligned}
P_{FA} &= \Pr(\varsigma = t-2 | \varsigma \geq t-2) \\
&\quad \cdot \Pr\left(\sup_{i\in[1,l_{t-1})} |\vartheta(i)| > \theta_\rho \,\middle|\, \sup_{i\in[1,l_{t-1})} |\vartheta(i)| < \rho^{(t-1)} \right) \\
&= \frac{\Pr(\varsigma = t-2)}{\Pr(\varsigma \geq t-2)} \\
&\quad \cdot \Pr\left(\sup_{i\in[1,l_{t-1})} |u(i)| > \frac{\theta_\rho}{\omega} \,\middle|\, \sup_{i\in[1,l_{t-1})} |u(i)| < \frac{\rho^{(t-1)}}{\omega} \right) \\
&= \frac{\Pr(\varsigma = t-2)}{\Pr(\varsigma \geq t-2)} \\
&\quad \cdot \frac{\Pr\left(\frac{\theta_\rho}{\omega} < \sup_{i\in[1,l_{t-1})} |u(i)| < \frac{\rho^{(t-1)}}{\omega} \right)}{\Pr\left(\sup_{i\in[1,l_{t-1})} |u(i)| < \frac{\rho^{(t-1)}}{\omega} \right)} \\
&= \frac{\Pr(\varsigma = t-2)}{\Pr(\varsigma \geq t-2)} \\
&\quad \cdot \frac{\Pr\left(\sup_{i\in[1,l_{t-1})} |u(i)| > \frac{\theta_\rho}{\omega} \right) - \Pr\left(\sup_{i\in[1,l_{t-1})} |u(i)| > \frac{\rho^{(t-1)}}{\omega} \right)}{1 - \Pr\left(\sup_{i\in[1,l_{t-1})} |u(i)| > \frac{\rho^{(t-1)}}{\omega} \right)}
\end{aligned} \tag{18}$$

where $\rho^{(t-1)}$ denotes $\hat{\rho}$ obtained in the $(t-1)$th iteration, that is, $\rho^{(t-1)} = \left| \hat{\underline{h}}_{prj}(l_{t-1}) / \hat{\underline{h}}_{prj}(l_1) \right|$; $u(i)$ denotes the i.i.d. Gaussian process with zero mean and unit variance; $\Pr\left(\sup_{i\in[1,T]} |u(i)| > \gamma \right)$ represents the two-sided level crossing probability of $u(i)$ at a level γ in a given region $[1, T]$. Similar to [35], this probability can be approximated by

$$\Pr\left(\sup_{i\in[1,T]} |u(i)| > \gamma \right) \approx 1 - \exp\left(-\frac{T}{E(\lambda)} \right) \tag{19}$$

where λ denotes the interval between a down-crossing and the next adjacent up-crossing of $|u(i)|$ at a given level γ. $E(\lambda)$ is simulated using a computer generated white Gaussian vector. By fitting on the simulation results, $E(\lambda)$ can be modeled by $E(\lambda) = p_1 \exp(q_1 \cdot \gamma) + p_2 \exp(q_2 \cdot \gamma)$, where the values of p_1, q_1, p_2, and q_2 are shown in Table I. Substituting $E(\lambda)$ into Equation (19), and then substituting (19) into (18), the final expression of P_{FA} can be obtained.

Note that the false alarm is uniformly distributed within the region $[1, l_{t-1})$, and hence the average false alarm error is

$$\varepsilon_{FA} = \frac{l_{t-1}}{2} T_s' \tag{20}$$

Table I. Parameter values of the model of $E(\lambda)$.

Parameter	Value
p_1	0.2595
q_1	2.342
p_2	9.518e−5
q_2	4.677

Therefore, the absolute TOA estimation error (AE) contributed by false alarm is

$$\mathbf{AE}_{FA} = P_{FA} \cdot \varepsilon_{FA} \tag{21}$$

5.1.2. Missed detection error.

The first path has not yet been found by the previous $t-1$ iterations, that is, $\varsigma \geq t-1$. Then during the tth iteration, we need to guarantee that the iteration will continue. If $\theta_\rho > \hat{\rho}$, then the iteration will stop, and the TP found by the $(t-1)$th iteration will be regarded as the first path, resulting in missed detection error. The estimated relative amplitude during the tth iteration then can be represented as $\hat{\rho} = |\rho_s + \rho_n|$, where ρ_s denotes the relative amplitude of the TP, whose absolute value follows the distribution denoted by $f_\rho(\rho|\xi)$; ρ_n follows Gaussian distribution with zero mean and variance of $\omega^2 = \sigma_{avg}^2 / {a_{PP}}^2$. Because the distributions of ρ_s and ρ_n are both symmetric, we can just take the positive case of ρ_s into consideration, that is, $\rho_s = \rho$, and $\hat{\rho} = |\rho + \rho_n|$. Letting $z = \rho + \rho_n$, because ρ and ρ_n are independent, the probability density of z is

$$f_z(z|\xi) = \int_0^1 f_{\rho_n}(z-\rho) f_\rho(\rho|\xi) d\rho \tag{22}$$

The missed detection probability can be deduced as follows:

$$\begin{aligned}
P_{MD} &= \Pr(\varsigma \geq t-1 | \varsigma \geq t-2) \\
&\quad \cdot \Pr\left(|z| < \theta_\rho \,\middle|\, |z| \leq \rho^{(t-1)}, \text{ and } \xi = t-1 \right) \\
&= \frac{\Pr(\varsigma \geq t-1)}{\Pr(\varsigma \geq t-2)} \cdot \frac{\Pr(|z| < \theta_\rho | \xi = t-1)}{\Pr(|z| \leq \rho^{(t-1)} | \xi = t-1)} \\
&= \frac{\Pr(\varsigma \geq t-1)}{\Pr(\varsigma \geq t-2)} \cdot \frac{\int_{-\theta_\rho}^{\theta_\rho} f_z(z|\xi = t-1) dz}{\int_{-\rho^{(t-1)}}^{\rho^{(t-1)}} f_z(z|\xi = t-1) dz} \\
&= \frac{\Pr(\varsigma \geq t-1)}{\Pr(\varsigma \geq t-2)} \\
&\quad \cdot \frac{\int_{-\theta_\rho}^{\theta_\rho} \int_0^1 f_{\rho_n}(z-\rho) f_\rho(\rho|\xi = t-1) d\rho dz}{\int_{-\rho^{(t-1)}}^{\rho^{(t-1)}} \int_0^1 f_{\rho_n}(z-\rho) f_\rho(\rho|\xi = t-1) d\rho dz}
\end{aligned} \tag{23}$$

1530867?, 2016, 17, Downloaded from https://onlinelibrary.wiley.com/doi/10.1002/wcm.2742 by University Of Waterloo, Wiley Online Library on [23/03/2026]. See the Terms and Conditions (https://onlinelibrary.wiley.com/terms-and-conditions) on Wiley Online Library for rules of use; OA articles are governed by the applicable Creative Commons License

The location of missed detection is indexed at l_{t-1}. Thus its arrival time difference relative to the PP is $\delta^{(t-1)} = (l_0 - l_{t-1})T_s'$. The true location of the first path is within the region $[1, l_{t-1})$, with time difference relative to the PP following the distribution denoted by $f_\delta(\delta|\varsigma)$. Therefore, the average missed detection error is

$$\begin{aligned}\varepsilon_{MD} = & \sum_{i=t-1}^{\infty} \left(\frac{\Pr(\varsigma = i)}{\Pr(\varsigma \geq t-1)} \cdot E\left(\delta \,\middle|\, \delta > \delta^{(t-1)}, \text{ and } \varsigma = i\right)\right) \\ & - \delta^{(t-1)} \\ = & \frac{1}{\Pr(\varsigma \geq t-1)} \\ & \cdot \sum_{i=t-1}^{\infty} \left(\Pr(\varsigma = i) \cdot \frac{\int_{\delta^{(t-1)}}^{\infty} \delta f_\delta(\delta|\varsigma = i) d\delta}{\int_{\delta^{(t-1)}}^{\infty} f_\delta(\delta|\varsigma = i) d\delta} \right) \\ & - \delta^{(t-1)}\end{aligned} \tag{24}$$

Then, the absolute TOA AE contributed by missed detection is

$$\mathbf{AE}_{MD} = P_{MD} \cdot \varepsilon_{MD} \tag{25}$$

5.2. Threshold setting criterion based on error minimization

Because of the effects of noise, it is possible that the searching process derails from the expected ideal track, that is, the derailment case may occur. In this case, some randomly located component may be detected as the first path when the iteration of MP-SB terminates. Let $AE_{derailment}$ denotes the absolute TOA AE for derailment case, and $P_{derailment}$ denote the corresponding occurrence probability. Then the expected TOA estimation AE during the current iteration can be expressed as

$$\begin{aligned}AE^{(t)} = & P_{derailment} \cdot AE_{derailment} + \\ & (1 - P_{derailment}) AE_{non\text{ - }derailment}\end{aligned} \tag{26}$$

where $AE_{non\text{ - }derailment}$ denotes the absolute TOA AE for non-derailment case. The expression of $AE_{non\text{ - }derailment}$ can be obtained based on the results of section VI-B, that is,

$$\begin{aligned}AE_{non\text{ - }derailment} &= AE_{FA} + AE_{MD} \\ &= P_{FA} \cdot \varepsilon_{FA} + P_{MD} \cdot \varepsilon_{MD}\end{aligned} \tag{27}$$

The optimal threshold can be selected such that $AE^{(t)}$ is minimized for the tth iteration, that is,

$$\theta_\rho^{opt} = \underset{0<\theta_\rho<\rho^{(t-1)}}{\arg\min} \; AE^{(t)} \tag{28}$$

Because the expressions of $P_{derailment}$ and $AE_{derailment}$ are very complex to derive, the optimal solution to the aforementioned problem cannot be obtained. As a sub-optimal solution, the threshold that simply minimizes the second part of $AE^{(t)}$ can be used, that is,

$$\theta_\rho^{sub-opt} = \underset{0<\theta_\rho<\rho^{(t-1)}}{\arg\min} \; ((1 - P_{derailment}) AE_{non\text{ - }derailment}) \tag{29}$$

The aforementioned compromise is reasonable because of the following facts:

- First, when the received signal SNR is high, the probability of derailment will be very low, so the first part of Equation (26) would be dominated and could be ignored.
- Second, when the received signal SNR is low, the final first path detection would be randomly located, so $AE_{derailment}$ is approximately independent of the threshold, and the first part of Equation (26) can also be omitted in the optimization problem.
- Third, the TOA estimation performance of using $\theta_\rho^{sub-opt}$ is comparable with that of using oracle threshold, which is justified in numerical results in Section 6.1.1.

Because $P_{derailment}$ is independent of the threshold, the problem can further be simplified as

$$\begin{aligned}\theta_\rho^{sub-opt} &= \underset{0<\theta_\rho<\rho^{(t-1)}}{\arg\min} \; AE_{non\text{ - }derailment} \\ &= \underset{0<\theta_\rho<\rho^{(t-1)}}{\arg\min} \; (P_{FA} \cdot \varepsilon_{FA} + P_{MD} \cdot \varepsilon_{MD})\end{aligned} \tag{30}$$

where P_{FA}, ε_{FA}, P_{MD} and ε_{MD} are given in Equations (18)–(25). It can be observed that $\theta_\rho^{(sub-opt)}$ is dependent on t (the current iteration times), ω (the relative noise power), $\rho^{(t-1)}$ (the relative amplitude of the previous found TP), and $\delta^{(t-1)}$ (the arrival time difference between the previous found TP and PP), where ω reflects the noise strength of the received ranging signal, and t, $\rho^{(t-1)}$ and $\delta^{(t-1)}$ reflect the individual channel characteristics of the current channel. Therefore, the threshold setting given by Equation (30) includes all key factors.

5.3. Case study

Different scenario would have different radio frequency propagation channel properties, so the statistics, that is, $\Pr(\varsigma)$, $f_\delta(\delta|\varsigma)$, $f_\rho(\rho|\xi)$, utilized in the error evaluation and threshold setting strategies are different, depending on specific environments. Here, we take the warehouse indoor as an example, where the IR-UWB propagation channel properties can be well characterized by the IEEE 802.15.4a channel models, to conduct case study for further verifying the threshold setting method.

A total of 1000 independent channel responses for CM1 and CM2 are generated individually. Table II shows the

15308677, 2016, 17, Downloaded from https://onlinelibrary.wiley.com/doi/10.1002/wcm.2742 by University Of Waterloo, Wiley Online Library on [23/03/2026]. See the Terms and Conditions (https://onlinelibrary.wiley.com/terms-and-conditions) on Wiley Online Library for rules of use; OA articles are governed by the applicable Creative Commons License

Table II. The result of $\Pr(\varsigma)$.

ς	0	1	2	3	4	≥5
CM1	0.229	0.363	0.246	0.107	0.04	0.015
CM2	0.101	0.268	0.291	0.203	0.101	0.036

Table III. The value of μ and v in equation (31) under different ς.

ς		1	2	3	4	≥5
CM1	μ	1.41	2.18	2.59	2.86	3.16
	v	1.13	0.81	0.66	0.56	0.45
CM2	μ	1.44	2.24	2.60	2.87	3.05
	v	1.10	0.79	0.64	0.68	0.60

Table IV. The value of a and b in equation (32) under different ξ.

ξ		1	2	3	4	≥5
CM1	a	2.91	2.70	2.83	2.33	1.66
	b	1.14	2.12	3.64	4.20	4.26
CM2	a	2.64	2.62	2.60	2.56	2.03
	b	1.12	2.31	3.72	4.62	4.75

result of $\Pr(\varsigma)$. For $\varsigma \geq 1$, that is, when the first path is not the strongest, the difference of arrival time between the first path and the PP satisfies $\delta > 0$. Statistic results show that $f_\delta(\delta|\varsigma)$ follows the lognormal distribution, that is,

$$f_\delta(\delta|\varsigma) = \frac{1}{\delta\sqrt{2\pi}v}\exp\left(-\frac{(\ln\delta-\mu)^2}{2v^2}\right), \quad \delta > 0 \quad (31)$$

where the values of μ and v, that is, the mean and variance of $\ln\delta$, vary with ς, as shown in Table III. As for $f_\rho(\rho|\xi)$, results show that it follows the Beta distribution, that is,

$$f_\rho(\rho|\xi) = \frac{1}{B(a,b)}\rho^{a-1}(1-\rho)^{b-1}, \quad 0 < \rho < 1 \quad (32)$$

where the value of a and b vary with ξ, as show in Table IV.

With the aforementioned the statistic results, the detection threshold for each iteration of MP-SB, that is, $\theta_\rho^{sub-opt}$, could be dynamically calculated out by Equation (30). Take the case of "$t = 3, \delta^{(t-1)} = 10\,\text{ns}$" as an example, the values of $\theta_\rho^{sub-opt}$ at different combinations of ω and $\rho^{(t-1)}$ are calculated and plotted in Figure 5. It can be seen that $\theta_\rho^{sub-opt}$ monotonically increases with ω and $\rho^{(t-1)}$.

We can further take a qualitative analysis on the impact of parameter AEs. With the assumption of non-derailment matching-pursuit, each tip path will be located precisely. Therefore, $\delta^{(t-1)}$, which indicates the location of the last found TP, can be accurately estimated. Furthermore, the parameter t represents the current iteration times, so it has

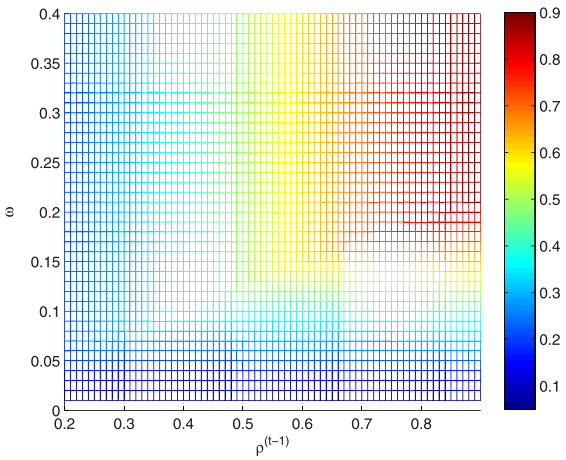

Figure 5. $\theta_\rho^{sub-opt}$ with respect to ω and $\rho^{(t-1)}$ when $t = 3$, $\delta^{(t-1)} = 10\,\text{ns}$.

no AEs. We thus can focus on the impact of AEs of ω and $\rho^{(t-1)}$ on the sub-optimum threshold.

- Let $\hat{\omega}$ be the estimate of ω. If $\hat{\omega}$ is larger than ω, then the probability of false alarms will increase. To suppress the false alarms so that the expected error decreases, the value of $\theta_\rho^{sub-opt}$ will be calculated out larger than what it should be.
- Let $\hat{\rho}^{(t-1)}$ be the estimate of $\rho^{(t-1)}$. If $\hat{\rho}^{(t-1)}$ is larger than $\rho^{(t-1)}$, then the probability of missed detections will decrease. The decrease of missed detection could be treated as a chance for suppressing the false alarms in the optimization procedure. Therefore, the calculated value of $\theta_\rho^{sub-opt}$ will also be larger than what it should be.

It can be concluded from the earlier analysis that the positive AE of both ω and $\rho^{(t-1)}$ would make $\theta_\rho^{sub-opt}$ larger than what it should be, as shown in Figure 5.

6. PERFORMANCE EVALUATIONS

In this section, we conduct performance evaluation by simulations as well as field data experiments, to demonstrate that the proposed ranging approach with IR-UWB can achieve high precision range estimates with far fewer samples than traditional methods using Nyquist sampling.

6.1. Simulations

The IEEE 802.15.4a CM1 and CM2 channel models, which can well characterize the indoor propagation properties, are used for ranging channel generation. Statistic results in Section 5.3, together with the proposed threshold setting criterion in Section 5.2, are used for first path threshold calculation for MP-SB. The detailed simulation settings are summarized in Table V. For each frame, the

15308677, 2016, 17, Downloaded from https://onlinelibrary.wiley.com/doi/10.1002/wcm.2742 by University Of Waterloo, Wiley Online Library on [23/03/2026]. See the Terms and Conditions (https://onlinelibrary.wiley.com/terms-and-conditions) on Wiley Online Library for rules of use; OA articles are governed by the applicable Creative Commons License

Table V. Simulation settings.

System parameter	$T_s' = 0.05$ns
Transmitter-related	Gaussian doublet with $T_p = 1$ns and pulse shaping factor of $T_p/2.2$ is used; $N_f = 20$, $T_f = 200$ns.
Channel-related	1000 different CIRs are generated for CM1 and CM2 individually, with TOAs uniformly distributed within [0, 100] ns.
Receiver-related	$D = 20$ and $M_e = 16$ (hence $N_D = 1$ and $M = 320^*$); $T_{prj} = 70$ ns; for each CIR, E_b/N_0 varies from 21 dB to 40 dB steped by 1 dB.

*Usually, $M \geq K \cdot \log(N)$ or $M \geq 4K$ measurements are needed to perfectly reconstruct the projected signal. Assuming that the resolvable multipath condition holds (i.e., $|\tau_i - \tau_j| \geq T_p \ \forall i \neq j$), the relax value of M for reconstruction can be calculated as $M \geq 4 \cdot T_{prj}/T_p = 280$. Here we choose a slightly larger value as $M = 320$ to guarantee the successful execution of MP-SB algorithm. The performance of MP-SB with respect to M is not discussed in this paper, because it is not hard to know that the algorithm performs better with larger M.

number of compressed samples is set as $M_e = 16$, and hence the equivalent sampling rate of the receiver can be easily calculated as $F_s = M_e/T_f = 80$ Msps, which is far fewer than the Nyquist rate. We will first validate the effectiveness of the proposed threshold setting method, and then compare the performance of MP-SB with traditional TOA estimation algorithms to show that even with low rate sampling, high precision ranging results can still be obtained.

6.1.1. Effectiveness of the proposed sub-optimal threshold setting method.

The performance of MP-SB with oracle threshold is simulated and compared with the proposed sub-optimal threshold, as shown in Figure 6. The oracle threshold is set with the prior knowledge of the location of the first path, that is, it enables the algorithm to terminate at the iteration that has the best detection. Specifically, the values of the oracle thresholds used in MP-SB are set as follows. During the tth iteration, comparing $\varepsilon^{(t-1)} = \left|\delta^{(t-1)} - \delta\right|$ with $\varepsilon^{(t)} = \left|\delta^{(t)} - \delta\right|$, if $\varepsilon^{(t)}$ is larger, then set θ_ρ^{oracle} within the region $(\rho^{(t)}, \rho^{(t-1)})$ to stop the iteration; otherwise, set θ_ρ^{oracle} within the region $(0, \rho^{(t)})$ to continue the iteration. It can be observed that the performance of using sub-optimal threshold is worse than that of using oracle threshold on the order of 5 dB from low-to-moderate SNR regions, because the oracle threshold values can hardly be achieved with any practical threshold setting strategy. As SNR increases, the performance gap between the two methods shrinks. This is mainly because that the probability of derailment case decreases and both the two methods will approach the performance lower bound that is determined by the virtual sampling interval. Because MP-SB with oracle threshold serves as the performance benchmark, the proposed threshold setting method has been proved to be very effective.

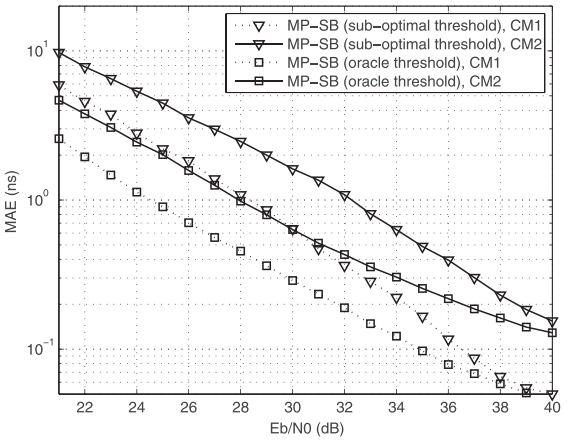

Figure 6. Comparison of the performance of matching-pursuit search-back (MP-SB) with the proposed sub-optimal threshold to that with oracle threshold. MAE, mean estimation error.

6.1.2. Comparison with Traditional time-of-arrival estimation algorithms.

The equivalent sampling rate of the receiver can be calculated as $F_s = M_e/T_f = 80$ Msps. This rate is extremely low for traditional IR-UWB ranging system, so only energy detection-based approaches can be used. The **E**nergy **D**etection based **T**hreshold **C**omparison, using **Kurtosis** as the threshold setting metric (ED-TC-Kurtosis) algorithm proposed in [18] is one of the most efficient ones, whose lower bound is known as $0.25/F_s = 3.125$ ns. The performance of MP-SB and ED-TC-Kurtosis under different SNRs is shown in Figure 7. It can be seen that when $E_b/N_0 > 24$ dB under CM1 (or $E_b/N_0 > 27$ dB under CM2), the mean AE (MAE, that is, the mean absolute TOA AEs over the 1000 ranging channels) of MP-SB decreases to below 3 ns, better than the lower bound barrier of the traditional energy detection based TOA estimation algorithm;

15308677, 2016, 17, Downloaded from https://onlinelibrary.wiley.com/doi/10.1002/wcm.2742 by University Of Waterloo, Wiley Online Library on [23/03/2026]. See the Terms and Conditions (https://onlinelibrary.wiley.com/terms-and-conditions) on Wiley Online Library for rules of use; OA articles are governed by the applicable Creative Commons License

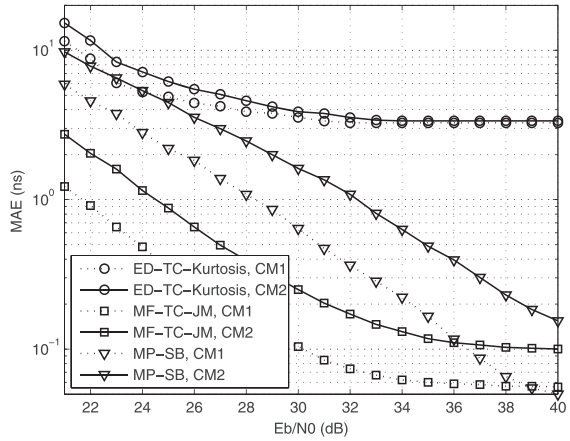

Figure 7. Performance comparison of matching-pursuit search-back (MP-SB), Energy Detection based Threshold Comparison, using Kurtosis as the threshold setting metric (ED-TC-Kurtosis), and Match-Filtering based Threshold Comparison using a Joint-Metric for threshold setting (MF-TC-JM). MAE, mean estimation error.

when $E_b/N_0 > 28$ dB under CM1 (or $E_b/N_0 > 32$ dB under CM2), the mean AE even decreases to below 1 ns.

Figure 7 also shows the performance of the **M**atch-**F**iltering based **T**hreshold **C**omparison using a **J**oint-**M**etric for threshold setting (MF-TC-JM) algorithm proposed in [14], which is a highly efficient coherent TOA estimation algorithm for traditional ranging systems. Note that traditional coherent algorithms including MF-TC-JM actually cannot work at low sampling rate as 80 Msps. To make the MF-TC-JM algorithm functioning, the sampling rate adopted in MF-TC-JM simulations is set to be the same as the virtual sampling rate under the CS framework, that is, $F_s' = 1/T_s' = 20$ Gsps. It can be seen that when SNR is sufficiently high (e.g., $E_b/N_0 > 38$ dB under CM1), MP-SB has approximately the same performance as MF-TC-JM, which verifies the efficiency of MP-SB. In addition, we can see that when the SNR is not so high, MP-SB performs worse than MF-TC-JM on the order of 6∼8 dB, which is mainly because the process of compressed sampling has systematical SNR loss [36]. How to mitigate or combat this systematical SNR loss will be our future work.

It is worth noting that the earlier simulation results are highly dependent on the ranging environments because the statistical results reflecting the propagation properties will vary when environment changes. For example, when the ranging or localization scenarios are changed to outdoor rural places, the results presented in Section 5.3 will change, and consequently the ranging performance at different SNR levels changes too, different from that shown in Figures 6 and 7. However, the effectiveness of the proposed ranging method we demonstrate here remain the same.

6.2. Field data experiments

To further validate the proposed approach, we carried out some indoor experimental tests. The experiment setup is shown in Figure 8. Details of the transceiver hardware design can be referred from [37]. At the transmitter, Gaussian pulse with width of $T_p = 1$ ns is generated periodically. The frame duration and number of frames are set as $T_f = 384$ ns and $N_f = 20$, respectively. At the receiver, the arrival signal is first sampled by a 2 Gsps ADC, then feed into the FPGA back-end, where TOA estimation is performed using the ED-TC-Kurtosis algorithm. We also put a digital oscilloscope with sampling rate of 25 Gsps at the receiver front-end to generate the high-speed virtual sampled sequence, which is then feed into a computer workstation where compressed samples are generated and processed by the proposed MP-SB algorithm. For each frame, $M = 200$ compressed samples are generated with $T_{prj} = 100$ ns, using a pseudo random matrix. The sampling rate of MP-SB can thus be calculated as $M/T_f =$

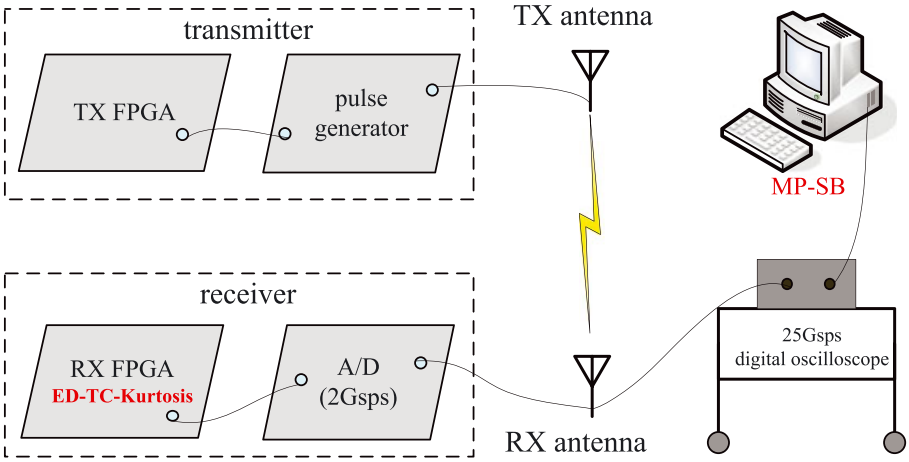

Figure 8. Experiment setup. A/D, analog-to-digital; ED-TC-Kurtosis, Energy Detection based Threshold Comparison, using Kurtosis as the threshold setting metric; FPGA, Field-Programmable Gate Array; MP-SB, matching-pursuit search-back.

15308677, 2016, 17, Downloaded from https://onlinelibrary.wiley.com/doi/10.1002/wcm.2742 by University Of Waterloo, Wiley Online Library on [23/03/2026]. See the Terms and Conditions (https://onlinelibrary.wiley.com/terms-and-conditions) on Wiley Online Library for rules of use; OA articles are governed by the applicable Creative Commons License

0.52 Gsps. Both the transmitter and receiver are placed in a meeting room with size of 8m×8m, and the in-between distance ranges from 1.2 to 4.8 m at the step of 0.6 m, all with line-of-sight condition. For each of the receiver locations, the range estimation results of ED-TC-Kurtosis and MP-SB are obtained by averaging over 40 times of ranging experiments and shown in Figure 9. It can be seen that with much lower sampling rate, MP-SB has achieved more accurate ranging results than the ED-TC-Kurtosis algorithm.

The experimental field data in [13] are also used for analysis. There are 17 sets of data (collected at Location 2∼18, respectively) in total, and all are collected under non line-of-sight situations. We process each data set as the virtual sampled form of the received ranging signal, with $T_f = 400$ ns; the virtual sampling rate thus equals to the sampling rate of the digital oscilloscope used in the experiments (that is 20.48 Gsps). Setting $T_{prj} = 100$ ns, $M = 400$, the signal within the projection interval can be measured using a pseudo random matrix, generating M compressed samples. Using these compressed samples as the input of the MP-SB algorithm, we can get the ranging results for each location, as shown in Figure 10. For comparison, the results in [13], which are obtained by generalized maximum likelihood based CLEAN algorithm, are also shown in Figure 10. It can be seen that the proposed approach achieves approximately the same performance, but the sampling rate is only $M/T_f = 1$ Gsps, far lower than the 20.48 Gsps rate required by [13].

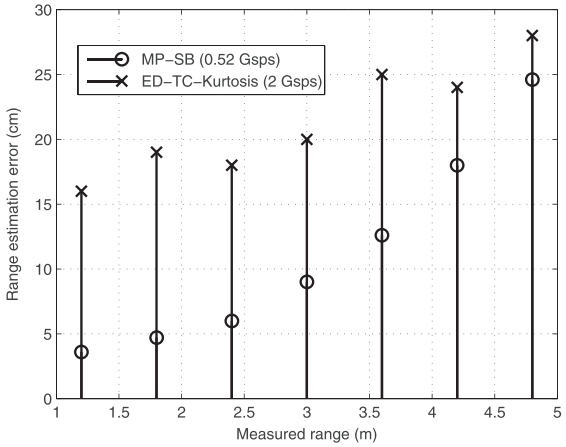

Figure 9. The results of field data experiments. ED-TC-Kurtosis, Energy Detection based Threshold Comparison, using Kurtosis as the threshold setting metric; MP-SB, matching-pursuit search-back.

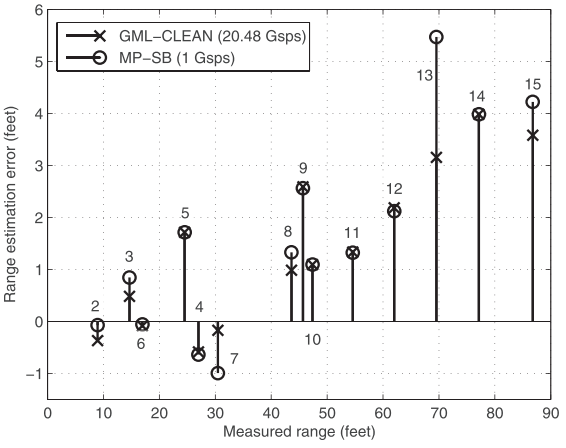

Figure 10. The results of test on experimental data by [13]. GML-CLEAN, generalized maximum likelihood based CLEAN algorithm; MP-SB, matching-pursuit search-back.

7. CONCLUSIONS AND FUTURE WORK

In this work, a high precision ranging approach with IR-UWB has been proposed under the emerging CS framework. The fundamental challenges with signal sampling and first path detection has been efficiently tackled by the proposed approach. An analog front-end architecture with parallel random demodulating channels has been presented for low-rate sampling the received IR-UWB ranging signal. Based on the compressed samples, the signal arrival time is estimated using the proposed MP-SB algorithm, whose general idea is to detect the first path by matching-pursuit with backward search from the peak path. Meanwhile, a threshold setting method that can dynamically adjust the detection threshold in each iteration for the MP-SB algorithm has been proposed to asymptotically minimize the averaged detection errors. Extensive simulations and field data experiments have shown that the proposed approach can achieve highly accurate ranging results but with far fewer samples, compared with traditional Nyquist sampling-based ranging approaches.

For the future work, the quasi-static characteristic of IR-UWB channel will be considered to mitigate the SNR loss. We also consider to explore measurement waveform for improving the efficiency of signal energy collection, which can be updated based on feedback information.

ACKNOWLEDGEMENTS

This research has been sponsored in part by the National Natural Science Foundation of China (Grant No. 61001092, 61371102) and the Natural Sciences and Engineering Research Council of Canada.

REFERENCES

1. Su Z, Xu Q, Qi Q. Big data in mobile social networks: a QoE oriented framework. *IEEE Network* 2016; **30**(1): 52–57.
2. Cong L, Zhuang W. Hybrid TDOA/AOA mobile user location for wideband CDMA cellular systems. *IEEE*

15308677, 2016, 17, Downloaded from https://onlinelibrary.wiley.com/doi/10.1002/wcm.2742 by University Of Waterloo, Wiley Online Library on [23/03/2026]. See the Terms and Conditions (https://onlinelibrary.wiley.com/terms-and-conditions) on Wiley Online Library for rules of use; OA articles are governed by the applicable Creative Commons License

Transactions on Wireless Communications 2002; **1**(3): 439–447.

3. Liu K, Lim HB, Frazzoli E, Ji H, Lee VCS. Improving positioning accuracy using GPS pseudorange measurements for cooperative vehicular localization. *IEEE Transactions on Vehicular Technology* 2014; **63** (6): 2544–2556.
4. Du J, Barth MJ. Next-generation automated vehicle location systems: positioning at the lane level. *IEEE Transactions on Intelligent Transportation Systems* 2008; **9**(1): 48–57.
5. Rose C, Britt J, Allen J, Bevly D. An integrated vehicle navigation system utilizing lane-detection and lateral position estimation systems in difficult environments for GPS. *IEEE Transactions on Intelligent Transportation Systems* 2014; **15**(6): 2615–2629.
6. Jia D, Lu K, Wang J, Zhang X, Shen X. A survey on platoon-based vehicular cyber-physical systems. *IEEE Communications Surveys and Tutorials* 2016; **18** (1): 263–284.
7. Cong L, Zhuang W. Non-line-of-sight error mitigation in mobile location. *IEEE Transactions on Wireless Communications* 2005; **4**(2): 560–573.
8. Wymeersch H, Lien J, Win MZ. Cooperative localization in wireless networks. *Proceedings of the IEEE* 2009; **97**(2): 427–450.
9. Efatmaneshnik M, Alam N, Kealy A, Dempster AG. A fast multidimensional scaling filter for vehicular cooperative positioning. *Journal of Navigation* 2012; **65**(2): 223–243.
10. Alam N, Balaei AT, Dempster AG. Relative positioning enhancement in VANETs: a tight integration approach. *IEEE Transactions on Intelligent Transportation Systems* 2013; **14**(1): 47–55.
11. Dardari D, Conti A, Ferner U, Giorgetti A, Win MZ. Ranging with ultrawide bandwidth signals in multipath environments. *Proceedings of the IEEE* 2009; **97** (2): 404–426.
12. MacGougan G, O'Keefe K, Klukas R. Tightly-coupled GPS/UWB integration. *Journal of Navigation* 2010; **63** (1): 1–22.
13. Lee J-Y, Scholtz R. Ranging in a dense multipath environment using an UWB radio link. *IEEE Journal on Selected Areas in Communications* 2002; **20** (9): 1677–1683.
14. Wu S, Zhang Q, Fan R, Zhang N. Match-filtering based TOA estimation for IR-UWB ranging systems, Crete Island, Greece.
15. Xu AY-Z, Au EKS, Wong AK-S, Wang Q. A novel threshold-based coherent TOA estimation for IR-UWB systems. *IEEE Transactions on Vehicular Technology* 2009; **58**(8): 4675–4681.
16. Candes E, Tao T. Near-optimal signal recovery from random projections: universal encoding strategies?. *IEEE Transactions on Information Theory* 2006; **52** (12): 5406–5425.
17. Donoho DL. Compressed sensing. *IEEE Transactions on Information Theory* 2006; **52**(4): 1289–1306.
18. Guvenc I, Sahinoglu Z. Threshold selection for UWB TOA estimation based on kurtosis analysis. *IEEE Communications Letters* 2005; **9**(12): 1025–1027.
19. Stoica L, Rabbachin A, Oppermann I. A low-complexity noncoherent IR-UWB transceiver architecture with TOA estimation. *IEEE Transactions on Microwave Theory and Techniques* 2006; **54** (4): 1637–1646.
20. Dardari D, Chong C-C, Win M. Threshold-based time-of-arrival estimators in UWB dense multipath channels. *IEEE Transactions on Communications* 2008; **56** (8): 1366–1378.
21. Ding H, Liu W, Huang X, Zheng L. First path detection using rank test in IR-UWB ranging with energy detection receiver under harsh environments. *IEEE Communications Letters* 2013; **17**(4): 761–764.
22. Paredes J, Arce G, Wang Z. Ultra-wideband compressed sensing: channel estimation. *IEEE Journal on Selected Topics in Signal Processing* 2007; **1** (3): 383–395.
23. Cohen KM, Attias C, Farbman B, Tselniker I, Eldar YC. Channel estimation in UWB channels using compressed sensing. In *Proc. of IEEE ICASSP'14*, Florence, Italy, 2014; 1966–1970.
24. Zhang P, Hu Z, Qiu R, Sadler B. A compressed sensing based ultra-wideband communication system. In *Proc. of IEEE ICC'09*, Dresden, Germany, 2009; 1–5.
25. Yao H, Wu S, Zhang Q, Wang Y. A compressed sensing approach for IR-UWB communication. In *Proc. of CMSP'11*, Guilin, China, 2011; 3–7.
26. Jin B, Zhang S, Pan J, Lin X. Pre-coding based compressed sensing UWB communication system for bursty applications. In *Proc. of IEEE GlobeCom'11*, Houston, USA, 2011; 1–5.
27. Wu J, Wang W, Liang Q, Wu X, Zhang B. Compressive sensing-based signal compression and recovery in UWB wireless communication system. *Wireless Communications and Mobile Computing* 2014; **14** (13): 1266–1275.
28. Shi G, Lin J, Chen X, Qi F, Liu D, Zhang L. UWB echo signal detection with ultra-low rate sampling based on compressed sensing. *IEEE Transactions on Circuits and Systems II: Express Briefs* 2008; **55**(4): 379–383.
29. Whitelonis N, Ling H. High-resolution radar imaging through a pipe via MUSIC and compressed sensing. *IEEE Transactions on Antennas and Propagation* 2013; **61**(6): 3252–3260.

15308677, 2016, 17, Downloaded from https://onlinelibrary.wiley.com/doi/10.1002/wcm.2742 by University Of Waterloo, Wiley Online Library on [23/03/2026]. See the Terms and Conditions (https://onlinelibrary.wiley.com/terms-and-conditions) on Wiley Online Library for rules of use; OA articles are governed by the applicable Creative Commons License

30. Chen N, Wu S, Li Y, Cao B. Compressed sensing enabled narrowband interference mitigation for IR-UWB systems. In *Proc. of WCSP'13*, Hangzhou, China, 2013; 1–5.
31. Needell D, Tropp J. CoSaMP: iterative signal recovery from incomplete and inaccurate samples. *Applied and Computational Harmonic Analysis* 2009; **26** (3): 301–321.
32. Molisch AF, Balakrishnan K, Cassioli D, Chong C-C, Emami S, Fort A, Karedal J, Kunisch J, Schantz H, Schuster U, Siwiak K. IEEE 802.15.4a channel model - final report. *Technical Report IEEE*, IEEE 802.15.4a channel modeling subgroup, 2005. Available: http://www.ieee802.org/15/pub/TG4a.html [accessed on November 9 2016].
33. Tropp J, Wakin M, Duarte M, Baron D, Baraniuk R. Random filters for compressive sampling and reconstruction. In *Proc. of IEEE ICASSP'06*, Toulouse, France, 2006; 872–875.
34. Kirolos S, Laska J, Wakin M, Duarte M, Baron D, Ragheb T, Massoud Y, Baraniuk R. Analog-to-information conversion via random demodulation. In *Proc. of IEEE Dallas Circuits and Systems Workshop (DCAS)*, Dallas, USA, 2006; 71–74.
35. Crandall S. First-crossing probabilities of the linear oscillator. *Journal of Sound and Vibration* 1970; **12**(3): 285–299.
36. Davenport MA, Laska JN, Treichler J, Baraniuk RG. The pros and cons of compressive sensing for wideband signal acquisition: noise folding vs. dynamic range. *IEEE Transactions on Signal Processing* 2012; **60**(9): 4628–4642.
37. Liu X, Wang H, Xu H. Design of a ultra-wideband pulse generator. *Journal of Telemetry, Tracking and Command* 2006; **27**(6): 55–58.

AUTHORS' BIOGRAPHIES

Shaohua Wu received the PhD degree from Harbin Institute of Technology in 2009, in communication engineering. From April 2009 to June 2011, he was a PostDoc at the Department of Electronics and Information Engineering, Shenzhen Graduate School of Harbin Institute of Technology (HITSZS), where he has been working till now. He has been an Associate Professor of HITSZS since July 2012. His current research interests include wireless image/video transmission, deep space communication, IR-UWB ranging/localization/communication, and 5G wireless transmission technologies.

Ning Zhang [S12, M16] earned the PhD degree from University of Waterloo in 2015. He received his BSc degree from Beijing Jiaotong University and the MSc degree from Beijing University of Posts and Telecommunications, Beijing, China, in 2007 and 2010, respectively. From May 2015 to April 2016, he was a postdoc research fellow at BBCR lab in University of Waterloo. He is now a postdoc research fellow at University of Toronto. His current research interests include next generation wireless networks, software defined networking, green communication, and physical layer security.

Haibo Zhou received the PhD degree in Information and Communication Engineering from Shanghai Jiaotong University, Shanghai, China, in 2014. He is currently a Post-Doctoral Fellow with the Broadband Communications Research (BBCR) Group, University of Waterloo. His current research interests include resource management and protocol design in cognitive radio networks and vehicular networks.

Qinyu Zhang received the PhD in 2003 from the University of Tokushima, Japan. From 1999 to 2003, he was an assistant professor at the University of Tokushima. Since 2005, he has been a full professor of Harbin Institute of Technology Shenzhen Graduate School and serves as the Dean of School of Electronic & Information Engineering. His research interests include wireless communications, cognitive radio, signal processing, and biomedical engineering. He is the founding chair of Communication Engineering Research Center supported by a couple of national research founding, including National Natural Science Foundation of China, National High Technology Research and Development Program, National Program on Key Basic Research Project, and so on.

Xuemin (Sherman) Shen [M97, SM02, F09] received the BSc (1982) degree from Dalian Maritime University (China) and the MSc (1987) and PhD degrees (1990) from Rutgers University, New Jersey (USA), all in electrical engineering. He is a Professor and University Research Chair, Department of Electrical and Computer Engineering, University of Waterloo, Canada. He was the Associate Chair for Graduate Studies from 2004 to 2008. Dr. Shens research focuses on resource management in interconnected wireless/wired networks, wireless network

15308677, 2016, 17, Downloaded from https://onlinelibrary.wiley.com/doi/10.1002/wcm.2742 by University Of Waterloo, Wiley Online Library on [23/03/2026]. See the Terms and Conditions (https://onlinelibrary.wiley.com/terms-and-conditions) on Wiley Online Library for rules of use; OA articles are governed by the applicable Creative Commons License

security, social networks, smart grid, and vehicular ad hoc and sensor networks. Dr. Shen served as the Technical Program Committee Chair/Co-Chair for IEEE Infocom14, IEEE VTC10 Fall, the Symposia Chair for IEEE ICC10, the Tutorial Chair for IEEE VTC11 Spring and IEEE ICC08, the Technical Program Committee Chair for IEEE Globecom07, the General Co-Chair for Chinacom07 and QShine06, the Chair for IEEE Communications Society Technical Committee on Wireless Communications, and P2P Communications and Networking. He also serves/served as the Editor-in-Chief for IEEE Network, Peer-to-Peer Networking and Application, and IET Communications; a Founding Area Editor for IEEE Transactions on Wireless Communications; an Associate Editor for IEEE Transactions on Vehicular Technology, Computer Networks, and ACM/Wireless Networks, and so on; and the Guest Editor for IEEE JSAC, IEEE Wireless Communications, IEEE Communications Magazine, and ACM Mobile Networks and Applications, and so on. Dr. Shen received the Excellent Graduate Supervision Award in 2006; the Outstanding Performance Award in 2004, 2007, and 2010 from the University of Waterloo; the Premiers Research Excellence Award (PREA) in 2003 from the Province of Ontario, Canada; and the Distinguished Performance Award in 2002 and 2007 from the Faculty of Engineering, University of Waterloo. Dr. Shen is a registered Professional Engineer of Ontario, Canada; an IEEE Fellow; an Engineering Institute of Canada Fellow; a Canadian Academy of Engineering Fellow; a Royal Society of Canada Fellow; and a Distinguished Lecturer of IEEE Vehicular Technology Society and Communications Society.

15308677, 2016, 17, Downloaded from https://onlinelibrary.wiley.com/doi/10.1002/wcm.2742 by University Of Waterloo, Wiley Online Library on [23/03/2026]. See the Terms and Conditions (https://onlinelibrary.wiley.com/terms-and-conditions) on Wiley Online Library for rules of use; OA articles are governed by the applicable Creative Commons License